Proceedings of the ASME 2022
ICE Forward Conference
ICEF2022
October 16-19, 2022, Indianapolis, Indiana

ICEF2022-91185

UNDERSTANDING AMMONIA/HYDROGEN FUEL COMBUSTION MODELING IN A QUIESCENT ENVIRONMENT

Amr Shaalan
Stony Brook University
Stony Brook, NY

Md Nayer Nasim
University of Massachusetts Lowell
Lowell, MA

J. Hunter Mack
University of Massachusetts Lowell
Lowell, MA

Noah Van Dam
University of Massachusetts Lowell
Lowell, MA

Dimitris Assanis
Stony Brook University
Stony Brook, NY

ABSTRACT

Ammonia and Hydrogen are attractive alternative fuels for a zero-carbon combustion solution that can rapidly decarbonize the transportation industry. Understanding the chemical behavior and combustion characteristics of these fuels individually, as well as blended together, is pivotal to ensuring their widespread adoption and utilization. Furthermore, in the era of computer-aided engineering, it is critical to evaluate our ability to computationally model the chemical reactivity of these two fuels and validate predictions of experimentally observed phenomena using multi-dimensional simulations. In this study, ammonia/hydrogen chemical kinetics mechanisms available from the research literature are investigated through 0-D, 1-D, and 3-D simulations. The 0-D and 1-D simulations were carried out to understand the ignition delay and laminar flame speeds, respectively, at different operating pressures and temperatures. 3-D simulations were also performed to test the fuels' behavior in a closed volume combustion chamber. The multi-dimensional computational results were compared against optically measured experimental data available in recent publications. Specifically, a comparison of unstretched flame speeds determined from stretched flame speeds of post-processed computational results is made. Lean and rich combustion limits have been computationally evaluated as well. Lastly, observed physical buoyancy effects were reproducible in a quiescent computational environment leading to increased confidence in using the evaluated chemical kinetics mechanisms for high-fidelity reciprocating piston engine computational research and development.

Keywords: Ammonia, Hydrogen, Combustion, Computational Fluid Dynamics, Chemical Kinetics Modelling.

NOMENCLATURE

S_N	Stretched Flame Speed
S_S	Unstretched Flame Speed
S_L	Laminar Flame Speed
ϕ	Equivalence Ratio
L_b	Burnt Gas Markstein Length
ε	Flame Stretch Rate
ρ_b	Burnt Gas Density
ρ_u	Unburnt Gas Density
T_u	Unburnt Gas Temperature
P	Pressure
A	Area of the Flame
r_{flame}	Flame Radius
r_{sch}	Schlieren Image Flame Radius
v_{H_2}	Hydrogen to Ammonia Fuel Ratio
τ_{ign}	Ignition Delay Time
dx, dy, dz	Cell Size in x,y,z
n	Cell Scale Factor

1. INTRODUCTION

Ammonia has attracted significant attention within the scientific community in recent years, not only as a carrier for hydrogen but also as a fuel on its own [1]–[4]. This special attention has been drawn from the rising need to decarbonize the fuels used for energy generation, in particular in the transportation sector for use in internal combustion engines [5]. The idea of using ammonia as a fuel in an internal combustion engine is decades old. One of the first recorded practical attempts appeared in 1936 and was patented in 1938 when ammonia was blended with ammonia-prepared hydrogen and nitrogen [6]. Shortly after, this device was used in 1942 as the first application on a large scale for about 100 vehicles, and for a bus in 1945 [7]. In 1967, Starkman et al. [8] compared the difference in the

performance of a spark-ignition engine fueled with iso-octane against ammonia. In that study, the authors showed that at low engine speeds (<1800 RPM) and stoichiometric conditions, ammonia's output indicated mean effective pressure (IMEP) was approximately 88% of the iso-octane's. When compared at their respective peak performance equivalence ratios, the relative IMEP ratio dropped to 80%. The authors also concluded that ammonia could not be used at higher engine speeds without the introduction of hydrogen. This was attributed to ammonia's low flame speed which impedes the engine's performance beyond 1800 RPM. In addition to those findings, ammonia was seen to require significantly higher ignition energy compared to usual hydrocarbon fuels [2]. Therefore, ammonia's implementation as a standalone fuel was deemed very difficult and is more appealing as a hydrogen carrier and a fuel to be blended with hydrogen.

Hydrogen is well known to have a very high flame speed as well as a wide flammability range [9], [10]. However, hydrogen has a very low volumetric energy density [11]. This in turn has posed challenges to hydrogen implementation in some fields, like transportation, as storage becomes very difficult. On the other hand, ammonia can be easily stored, and its production infrastructure is well-established. A single mole of ammonia is comprised of 17.8% of hydrogen by weight, which corresponds to 108 kg-H_2/m^3 for liquid ammonia at 20° C. This makes ammonia stand out as a hydrogen carrier against other hydrogen storage systems, e.g. metal hydrides which can only store up to 25 kg/m^3 [11]. It can therefore be said that hydrogen compensates for the shortcoming of ammonia in its combustion behavior, and ammonia offers a solution to hydrogen storage and production problems. Nonetheless, properly blending ammonia and hydrogen for combustion purposes requires a deep understanding of the chemical kinetics, as while their combustion with air can theoretically be clean and only produce water and nitrogen when fully combusted, this is not always the case as undesirable emissions such as NOx can be formed.

In order to understand the kinetics of ammonia, a deep base of experimental measurements is required. Pure ammonia and ammonia mixtures fuel experiments in the past few decades have laid the groundwork for advanced chemical kinetics models to validate against. Ronney et al. [12] attempted to study the chemical kinetics behavior of different fuels including ammonia/air and hydrogen/air. Pfahl et al. [13] carried out experiments on hydrogen, methane, ammonia, nitrous oxide, oxygen, and nitrogen mixtures to identify their flammability limits, ignition energy, and flame speeds. Tian et al. [14] developed experiments to understand the chemical kinetics of ammonia/methane/oxygen/argon mixtures and developed a chemical kinetics model at low pressure and stoichiometric equivalence ratio, ϕ. A more recent study by Hayakawa et al. [2] studied ammonia/air mixture flame speed, Markstein length, and flammability limits at different pressures. This study was further expanded by Ichikawa et al. [9] to include stoichiometric ammonia/hydrogen/air mixtures with different hydrogen content percentages. Mathieu et al. [15] also carried out a study to identify the ignition delay of ammonia/oxygen heavily-diluted in Argon, where different pressures, equivalence ratios, and Argon dilution percentages were reported and compared.

With respect to the chemical kinetics themselves, in 1983, the first comprehensive ammonia oxidation chemical kinetics model was developed and published consisting of 98 reactions [16]. Since then, significant work has been done to better understand the combustion behavior of ammonia. One of the most notable models is from Konnov and de Ruyck [17] which is a detailed mechanism with 129 species and 1231 reactions that involved a full H/N/O mechanism. The model underwent testing and correction for ammonia combustion in recent studies [2], [9], [18]–[21]. The model laid the grounds for more work toward a deeper understanding of the chemical kinetics needed for combustion modeling. More recent models by Otomo et al. [22] and Stagni et al. [23] offer accurate predictions of ammonia kinetics behavior. both models were developed from Song et al. [24], which were in turn developed from the model by Klippenstein et al. [25], who based their model on Miller et al. [26], which was derived from James A. Miller et al.'s original 1983 model.

In this work, a computational study was conducted comparing multiple chemical kinetics mechanisms to identify the relative strengths and weaknesses of the currently available mechanisms. The mechanisms were compared using 0-D and 1-D models in CHEMKIN-Pro [27] to get and compare the ignition delay and laminar flame speed, respectively, against available experimental data. The top-performing model was further investigated in a 3-D model of the constant volume combustion chamber experimental setup used in Ichikawa et al. [9] and Hayakawa et al. [2] using CONVERGE CFD [28]. Results of the 3-D simulations were visually compared against the experimental images, and quantitative comparisons were made against experimental laminar flame speed values. A deeper comparison of stretched and unstretched flame speeds, flame stretch rates, and Markstein lengths from the 3D simulations against experimental data from constant volume combustion chamber data was also included in this study.

2. MATERIALS AND METHODS

To fully understand the chemical kinetics behavior of the combustion of ammonia and ammonia/hydrogen combustion, comprehensive 0-D and 1-D studies of selected models available in the literature were performed, comparing these models against available experimental data from the literature. Both 0-D and 1-D studies were done in Chemkin-Pro. The 3-D analysis of the flame structure was done using CONVERGE CFD and was compared with the available 3-D flame images [2], [9]. The details of each of these models and the metrics used for comparison with relevant experimental data are given in the following sections.

2.1 Chemical Kinetics Models

Different models were included in this study for different purposes. For ammonia/air combustion, four (4) models were used for laminar flame speed calculations: Tian et al. [14] has 84 species and 703 reactions Song et al. [24] has 34 species and 204 reactions, Otomo et al. [22] has 32 species and 211 reactions, and Stagni et al. [23] has 31 species and 203 reactions. These models were published in 2009, 2016, 2017, and 2020, respectively. These models were selected in chronological order to see the improvement done over time in our understanding of the kinetics of ammonia/air combustion. Otomo et al. was selected for further analysis using 3-D CFD as it was seen to give the best laminar flame speed predictions compared to the experimental data. The two most recent models, Otomo et al. and Stagni et al., also included argon species which was necessary for ignition delay time analysis and were therefore chosen for the 0-D analysis.

For ammonia/hydrogen/air combustion, five (5) models were used for laminar flame speed calculations. Three (3) models that were also used for ammonia/air combustion, Otomo et al., Tian et al., and Stagni et al. In addition to Konnov [29], which consists of 127 species and 1207 reactions, and GRI-Mech 3.0 [30], which consists of 53 species and 325 reactions. Konnov et al. model was published in 2001 for ammonia and hydrogen oxidation in air. GRI-Mech 3.0 was not originally created for ammonia/hydrogen/air combustion but targeted natural gas combustion. Nonetheless, it was seen to provide good results in recent publications [2], [9] and was therefore included in this study for comparison. For further analysis for laminar flame speed-equivalence ratio dependence and ignition delay time, only Otomo et al. and Stagni et al. were used. Stagni et al. was seen to produce the best representation of the laminar flame speed at different ammonia/hydrogen fuel ratios but they both produced similar results for hydrogen laminar flame speed at different equivalence ratios. Therefore, Otomo et al. was used in CFD for consistency with the ammonia cases.

2.2 0-D Ignition Delay Model

Ignition delay was calculated in Chemkin-Pro using the 0-D closed homogenous reactor [27]. The results obtained by this model for ammonia were compared with the experiments performed by Mathieu et al. [15] where ammonia was tested in high argon dilution conditions of 99% argon and oxygen was used as the oxidizer. An equivalence ratio sweep was done over three (3) different initial pressures of 1.4 atm, 11 atm, and 30 atm. For hydrogen auto-ignition, data from Krejci et al. [31] of the autoignition of hydrogen in high (99%) argon dilution with oxygen. The equivalence ratio tested by Krejci et al. was 0.5 at 32 atm. In all of the experiments, the ignition delay time was determined by measuring the onset time of chemiluminescence emission of an excited state hydroxyl radical (OH*) from its time profile in a reflected shock wave [22]. For simulations, the temperature values over time were analyzed and the peak rate of change of the temperature in the domain was chosen to be the ignition time delay.

2.3 1-D Flame Speed Model

The laminar flame speed calculated in Chemkin-Pro was done using the Premixed Laminar Flame-Speed Calculation module in the Flame Simulators [27]. The calculations in this module are done in a 1-D domain with adaptive mesh refinement, the length of which was adjusted for each ammonia case to ensure convergence, this is due to the low reactivity and laminar flame speed of ammonia, especially near the lean and rich limits which required a longer length to reach final combustion products. For ammonia/hydrogen/air combustion, experimental data [9], [32]–[34] of the laminar flame speed of ammonia/hydrogen fuels at fuel fractions from 0 (pure ammonia) to 1 (pure hydrogen) were compared against chemical kinetics model predictions [14], [17], [22], [23], [30]. An equivalence ratio sweep was compared with experimental data by Krejci et al. [31]. All the flame speed runs were done at unburnt temperature of 298 K and pressure of 0.1 MPa.

2.4 3-D Chemical Kinetics Coupled CFD Model

A 3-D computational model was created in CONVERGE CFD to mimic the experimental setup shown by Hayakawa et a. and Ichikawa et al. [2], [9]. The geometry is a simple cylinder with an inner diameter of 270 mm and length of 410 mm, as shown in FIGURE 1, with two (2) electrodes spaced 2 mm apart at the center to ignite the mixture. In the computational model, the two (2) electrodes were removed and the spark was modeled as a spherical energy source at the center of the cylinder. The ignition energy was set at 2.8 J for all ammonia cases and was reduced linearly with the hydrogen volume content to reach 0.28 J for the 100% hydrogen case, following the same ignition energy methodology adopted in the experiments All cases were at initial pressure and temperature of 0.1 MPa and 298 K, respectively. The equivalence ratio and fuel composition were varied from case to case. For the pure ammonia cases, the equivalence ratios tested were 0.7, 0.8, 1.0, 1.1, 1.2, and 1.3. In addition, two (2) cases of hydrogen at a hydrogen:ammonia volumetric ratio of 0.4:0.6 and 1:0 (i.e. pure hydrogen) were included in this study

No turbulence model was used to simulate the laminar conditions. Fixed cell embedding was used to ensure the ignition and initial flame development were well captured. In addition, Adaptive Mesh Refinement (AMR) was used to make sure the flame front is well resolved as the flame propagates. The base grid cell size was 10 mm in all directions. For all runs, a spherical fixed cell embedding with scales six (6), five (5), and three (3) at radii of 5 mm, 10 mm, and 30 mm, respectively, centered at the spark location. CONVERGE CFD uses rectangular cells with each embedding level corresponding to dividing the cell in half in each direction. The embedding scale corresponds to the levels of embedding, equivalent to the variable n in Equation (1).

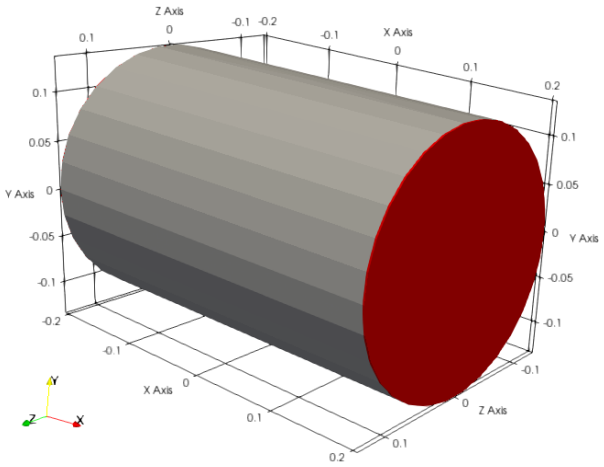

FIGURE 1. COMPUTATIONAL DOMAIN. UNITS ARE REPRESENTED IN METERS.

$$dx = \frac{dx_{base}}{2^n} \quad (1)$$

The AMR variables were temperature, with a sub-grid criterion of 1 K, and density, with a sub-grid criterion of 0.1 kg/m^3. For the pure ammonia runs, the embedding scales for both variables were set to 6, leading to a minimum cell size of dx = 0.15625 mm. For the hydrogen-blended cases, the embedding scales for both variables were set to 7, leading to a minimum cell of 0.078125 mm. The combination of temperature and density as variables for AMR was chosen to give enough resolution in the flame and the preheat zone, as shown in FIGURE 2. The initial cell count for all the runs was approximately 4×10^5, growing to 2×10^6 for the pure ammonia cases and 20×10^6 for the hydrogen-blended cases by the end of the simulations due to AMR as the flame grows. In addition, CONVERGE CFD uses an adaptive time-stepping algorithm based on local Courant–Friedrichs–Lewy (CFL) number and other stability limits. For all simulations, the maximum CFL was limited to 1. The minimum and maximum time step sizes were set to be 10 nanoseconds and 0.1 milliseconds, respectively. The pure ammonia cases took an average runtime of about 30 hours to simulate 80 ms, while the pure hydrogen cases took about 24 hours to simulate 2 ms.

The laminar flame speed and Markstein length were determined from the stretched flame speed and the stretch rate of the flame, which are given by Eqn. (2) and Eqn. (3), respectively. The plot of stretched flame speed vs. stretch rate was then used to evaluate the unstretched flame speed and the Markstein length by fitting a straight line through the resulting points, as shown in FIGURE 3, resulting in an equation of the form given by Eqn. (4) [35]. The unstretched flame speed was then used to get the laminar flame speed via Eqn. (5).

$$S_N = \frac{dr_{flame}}{dt} \quad (2)$$

$$\varepsilon = \frac{1}{\mathrm{A}} \cdot \frac{dA}{dt} \quad (3)$$

$$S_N = S_S - L_b \cdot \varepsilon \quad (4)$$

$$S_L = \frac{\rho_b}{\rho_u} \cdot S_s \quad (5)$$

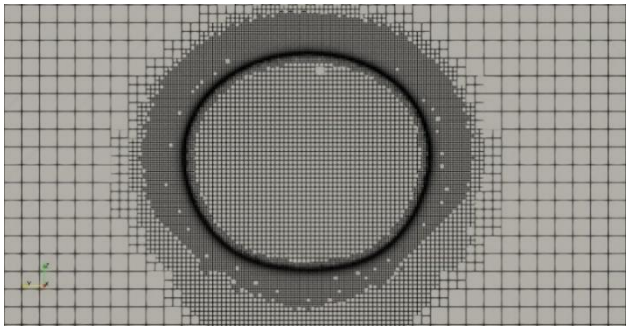

FIGURE 2. GRID REPRESENTATION WITH SOLUTION AND ADAPTIVE MESH REFINEMENT.

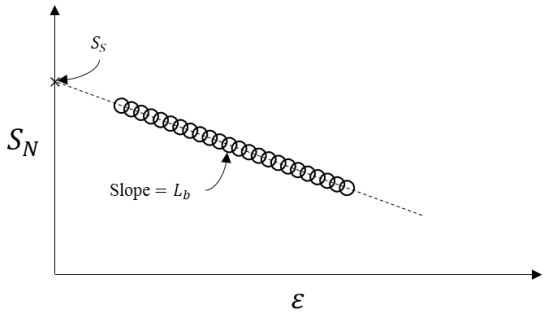

FIGURE 3. ILLUSTRATION OF S_S AND L_b EXTRACTION FROM EQUATION (4)

Accurately evaluating the radius of the flame is the key to accurately evaluating the laminar flame speed. Hayakawa et al. and Ichikawa et al. [2], [9] estimated the radius of the flame by evaluating the area of the shape the flame forms in the schlieren images and getting the radius of the circle that has the same area. Eqn. (3) can then be modified by substituting the area with a sphere's surface area, $A = 4\pi r_{sch}^2$.

$$\varepsilon = \frac{2}{\mathrm{r_{flame}}} \cdot \frac{dr_{flame}}{dt} \quad (6)$$

Eqn. (5) requires the densities of the burnt and unburnt mixtures to identify the laminar flame speed. Hayakawa et al. [2] and Ichikawa et al. [9] calculated the values shown in TABLE 1 using chemical equilibrium in CHEMKIN-PRO with the thermodynamic data of Tian et al. [14]. The same values were used in this study for all flame speed calculations to ensure a fair comparison.

To calculate the rate of change of the flame radius necessary for Eqn. (6) for the simulation results three (3) different methods

were used. These methods are explained in the following sections.

		$\rho_b\ (kg/m^3)$	$\rho_u\ (kg/m^3)$
ϕ	**0.8**	0.167	1.091
	1	0.146	1.074
	1.1	0.146	1.066
	1.2	0.148	1.058
x	**0.4**	0.139	1.002
	1	0.124	0.855

TABLE 1. DENSITIES USED FOR LAMINAR FLAME SPEED CALCULATION. ADAPTED FROM HAYAKAWA ET AL. [2] AND ICHIKAWA ET AL. [9].

2.4.1 Method I – Equivalent Area Method

In the experiments, the radius was identified as the radius of the circle with the same surface area as the shape formed by the flame in the schlieren images. The closest implementation of this method can be applied to the simulation results by projecting the coordinates of the cells on the flame surface onto the yz-plane and evaluating the area formed by the outermost cells. This area may then be used to define the radius of a circle with an equivalent area, as was done in the experiments. This method will henceforward be referred to in this work as the "Equivalent Area" method or method I.

2.4.2 Method II – Moving Center Method

An average radius can be evaluated by tracking the geometric center of the cells in the flame and then getting the average radius with respect to this center. Normally for faster flames, the center of the flame can be accurately assumed constant at the site of ignition. However, for slow-moving flames such as those for ammonia, the center can start shifting upwards through buoyancy effects. This method is expected to produce data with less variability as all the cells in all three (3) dimensions will be taken into consideration while averaging, which would dampen rapid changes to the radius, as opposed to the equivalent area method where the area in the 2-dimensional yz-plane is strongly affected by changes in the flame surface's shape. This method will hereinafter be referred to in this work as the "Moving Center" method or method II.

2.4.3 Method III – Image Processing Method

This method is based on an alternative experimental approach to calculate the flame speeds from image frames from an image sequence of numerical schlieren data. The images are converted into greyscale and then binarized to detect the edge of the expanding flame. Image processing and edge detection was performed with the image processing toolbox in MATLAB. The diameter of the propagating flame was calculated for each frame by multiplying the calibration factor (length per pixel) with the pixel value difference of two opposite edges on an axis. After identifying the region where the flame was expanding in a quasi-steady state, the instantaneous flame speed and stretch rate were calculated within that range for two consecutive images from the sequence using Equation (2) and Equation (6), respectively. This method will be referred to as the "Image Processing Method" method or method III in this work.

3. RESULTS AND DISCUSSION

3.1 Ammonia Combustion

Ammonia has a significantly lower laminar flame speed compared to other conventional fuels. FIGURE 4 shows the laminar flame speed of ammonia at different equivalence ratios. Ammonia's peak laminar flame speed at P = 0.1 MPa and T_u = 298 K occurs around ϕ = 1.1 with an approximate value of 7 cm/s. Iso-octane, under the same pressure and temperature, has more than four (4) times that speed with a peak laminar flame speed of approximately 30.4 cm/s occurring at around ϕ = 1.15 [33].

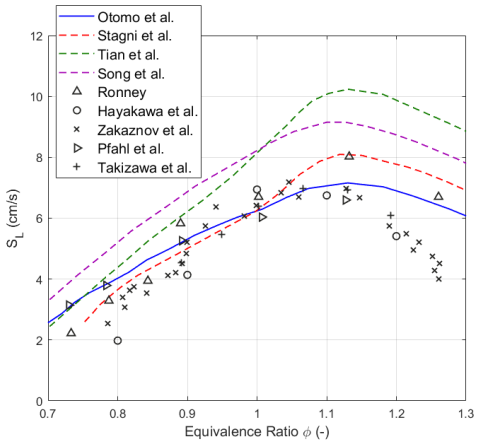

FIGURE 4. LAMINAR FLAME SPEED S_L VS EQUIVALENCE RATIO ϕ AT $P = 0.1\,MPa$ AND $T = 298\,K$. SIMULATION REPRESENTED BY LINES: OTOMO ET AL. [22], STAGNI ET AL. [23], TIAN ET AL. [14], SONG ET AL. [24]. EXPERIMENTAL DATA REPRESENTED BY MARKERS WITH NO LINES: RONNEY [12], HAYAKAWA ET AL. [2], ZAKAZNOV ET AL. [36], PFAHL ET AL. [13], TAKIZAWA ET AL. [37].

It can also be seen that the chemical kinetics models tend to over-predict the laminar flame speeds, in particular at rich conditions ($\phi > 1.0$). Nonetheless, the most recent models by Otomo et al. and Stagni et al. have a significantly higher accuracy when compared with older models like Tian et al. and Song et al.

The 0-D analysis of the ignition delay time of ammonia using Otomo et al. and Stagni et al. showed accurate results, with Stagni et al. giving results closer to the experiments done by Mathieu et al. while Otomo et al. slightly overestimated the ignition delay time. The consistency of the results is shown across different pressures of 1.4 atm, 11 atm, and 30 atm. The results are plotted in FIGURE 5. It is also important to note that in all of the experimental results shown here, the shortest ignition delay time is seen in lean conditions and the longest in rich conditions. This trend was also confirmed by the numerical models. Studies done on other fuels, such as iso-octane and

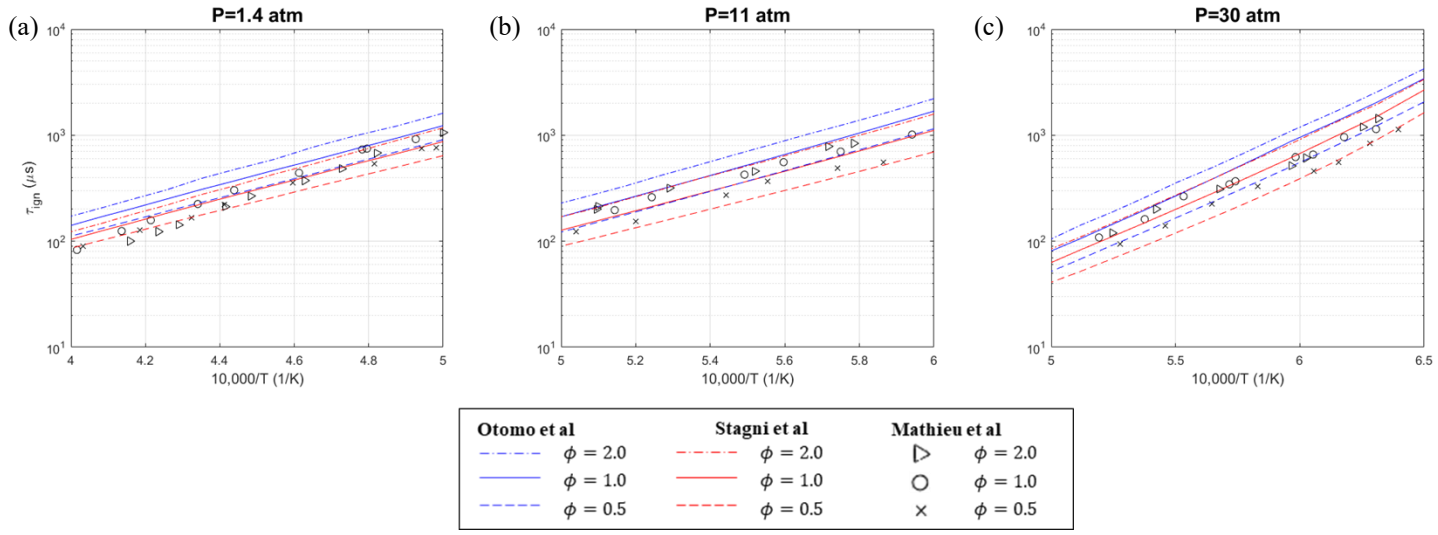

FIGURE 5. IGNITION DELAY TIME COMPARISON OF AMMONIA/AIR COMBUSTION BETWEEN EXPERIMENTAL VALUES BY MATHIEU ET AL. [15] AND 0-D MODELS USING CHEMICAL KINETICS MODELS FROM OTOMO ET AL. AND STAGNI ET AL. AT EQUIVALENCE RATIOS $\phi = 0.5, 1.0, 2.0$ AND INITIAL PRESSURE (A) $P = 1.4\ atm$ (B) $P = 11\ atm$ (C) $P = 30\ atm$.

surrogates, show the trend to be reversed [38], [39]. It is unclear why this is happening for ammonia combustion, but it would indicate that under internal combustion engine-like conditions zones with lower equivalence ratios in the cylinder, ammonia would be more susceptible to knocking.

The 3-D chemistry-coupled predictions are fairly close to the 1-D model for the lean and stoichiometric cases, as shown in FIGURE 6, regardless of the method used to calculate the flame radius. The lean flammability limit showed by Hayakawa et al. was also verified, where no flame propagation was achieved at $\phi = 0.7$. However, under richer conditions, the laminar flame speed extracted from the 3-D model was significantly lower than the 1-D model and slightly underpredicted the experimental values. However, it can be said that the laminar flame speeds from the CFD results are in good agreement with the experimental data across the equivalence ratios tested.

Comparing the different flame speed calculation methods directly, methods I and II are generally in good agreement and produced similar results. Method III consistently gave a higher estimation of the laminar flame speed. The main reason for this difference is believed to be because of the relatively fewer number of frames from the CFD runs. This method is more appropriate for the higher frame available experimentally when using high-speed cameras. While CFD simulations take much smaller time steps, data is saved at lower frequencies due to the large size of CFD datasets. To further illustrate the differences between the flame speed calculation methods, the stretched flame speed versus stretch rate along with the linear extrapolation used to determine the unstretched flame speed is plotted in FIGURE 7. Methods I and II have very similar data, with the main difference being that Method I produces noisier data, i.e. there is greater scatter between the data points. Method III, on the other hand, calculates higher stretched flame speeds, which resulted in greater unstretched flame speeds and the laminar flame speed differences that can be seen in FIGURE 6.

The development of chemical kinetics models is mainly done through a 1-D approach where the curvature is not accounted for. Yet, in most experiments, a flame curvature is often unavoidable. Therefore, a correction to get the unstretched flame speed is necessary. This correction's accuracy is tested only in 3-D analysis where the curvature is accounted for. FIGURE 7 illustrates the difference in determining the unstretched flame speed and burned gas Markstein length from the stretched flame speed and stretch rate of the stoichiometric ammonia case. The difference in the slope and y-intercept is most clear for method III. Nonetheless, an argument can be made about whether the linear approximation put forward by Markstein [35] is representative of the true nature of the flame in this case, specifically in the presence of visual comparison with the experimental data.

FIGURE 8 shows the comparison of the Markstein length calculated from the CFD runs and the experiments. The experiments showed a significant difference between the leanest and richest cases, while in the CFD the Markstein length did not change significantly. This indicates that the actual flame speed in more realistic flames where curvature and different shapes are occurring will not be well predicted, especially in non-stoichiometric compositions. It can therefore be said that the CFD Markstein length trend was not representative of the experimental results.

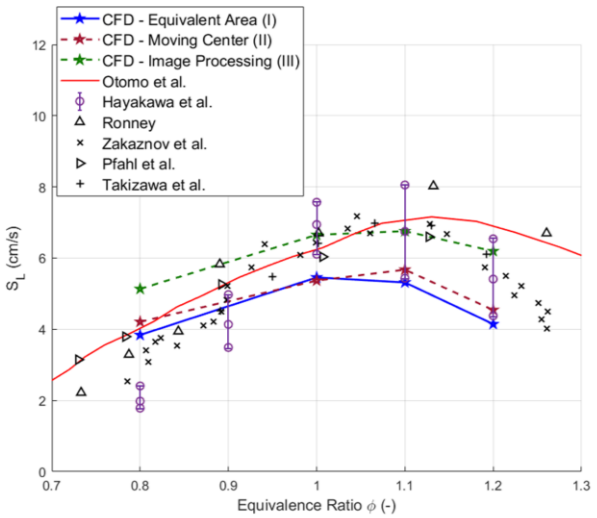

FIGURE 6. LAMINAR FLAME SPEED S_L VS EQUIVALENCE RATIO ϕ 3-D CFD ANALYSIS RESULTS OBTAINED WITH OTOMO ET AL. [22] USING METHOD I, II, AND III WITH 1-D MODEL USING OTOMO ET AL. (SOLID LINE), EXPERIMENTAL DATA BY HAYAKAWA ET AL. [2] (WITH UNCERTANITY), RONNEY [12], ZAKAZNOV ET AL. [36], PFAHL ET AL. [13], AND TAKIZAWA ET AL.[37]. $T = 298\ K$ AND $P = 0.1\ MPa$.

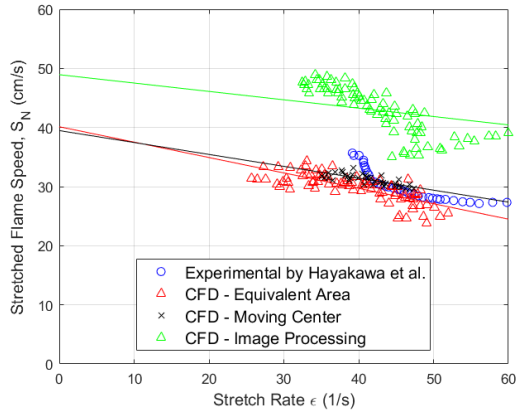

FIGURE 7. STRETCHED FLAME SPEED S_N VS. STRETCH RATE ϵ COMPARISON OF COMPUTATIONAL AND EXPERIMENTAL RESULTS BY HAYAKAWA ET AL. [2] OF AMMONIA AT $\phi = 1$, $P = 0.1\ MPa$ AND $T_u = 298\ K$.

Modeling of the ignition has proved to be very challenging for the case of ammonia. FIGURE 9 shows the comparison of the flame surface in CFD and the experiments. For the case where the laminar flame speed was closest to the experimental values, it can be seen that the flame was slower during the initial phase and until t = 10 ms. Afterward, the flame radius visually looks to be growing at the same rate as the experiments, thus, leading to the same flame speed and not the exact flame radius at a given time. It can also be verified that the buoyancy effects were captured for slower flames. This is most clear in the lean case at $\phi = 0.8$ where a strong agreement with the flame shape is shown. Similar to the stoichiometric case the ignition-affected initial phase of the flame was also slower than in the experiments. However, as the chemical kinetics model had a faster laminar flame speed than the experiments done by Hayakawa et al., the flame was able to catch up to the experiments and resulted in a similar flame shape at a given time.

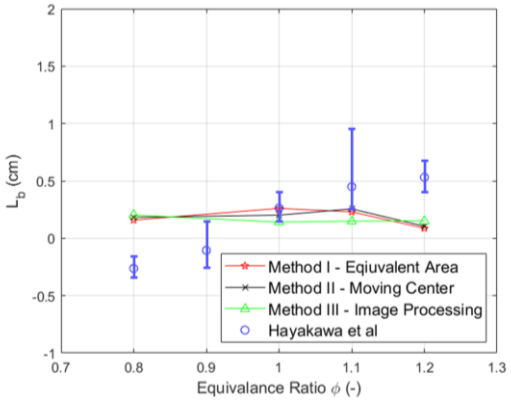

FIGURE 8. MARKSTEIN LENGTH L_b VS EQUIVALENCE RATIO ϕ COMPARISON OF 3-D CFD ANALYSIS OBTAINED WITH OTOMO ET AL. [22] AND EXPERIMENTAL RESULTS BY HAYAKAWA ET AL. [2] OF AMMONIA AT $\phi = 1$, $P = 0.1\ MPa$ AND $T_u = 298\ K$

3.1 Ammonia/Hydrogen Combustion

The introduction of hydrogen to ammonia enhances the combustion of ammonia dramatically. FIGURE 10 plots the value of the laminar flame speed with different volumetric hydrogen to ammonia fuel fractions at a constant equivalence ratio of 1. The laminar flame speeds predicted by the chemical kinetics models show very accurate results compared to the experimental data. GRI-Mech 3.0 [30] gives the least accurate predictions, this is expected as it is developed for natural gas combustion.

Unlike ammonia/air combustion, ammonia/hydrogen/air combustion results in a faster flame that develops more quickly, is less dependent on the spark event, and is virtually unaffected by buoyancy effects. From the visual comparison of the flame structure in the experiments and the CFD results in FIGURE 14, it can be seen that the flame development, structure, and radius at all given times are very accurate at $v_{H_2} = 0.4$ while the $v_{H_2} = 1$ (i.e. pure hydrogen) case's ignition appears to be slower than the experiments. It is also important to note that, consistently ammonia/air combustion, the 3-D analysis with Otomo et al. underestimated the laminar flame speed compared to the 1-D model. This shows the difficulty of estimating the unstretched flame speed from the stretched laminar flame speed, whereas in the 3-D analysis the estimation of the shape of the flame surface plays a pivotal role in the estimation of the laminar flame speed. FIGURE 11 shows this relationship to be accurate at $v_{H_2} = 0$ and 0.4 but is overestimated for the pure hydrogen case. It can therefore be said that, for the pure hydrogen case, the significantly lower stretched flame speed (visually shown in FIGURE 14) resulted in the slower final laminar flame speed.

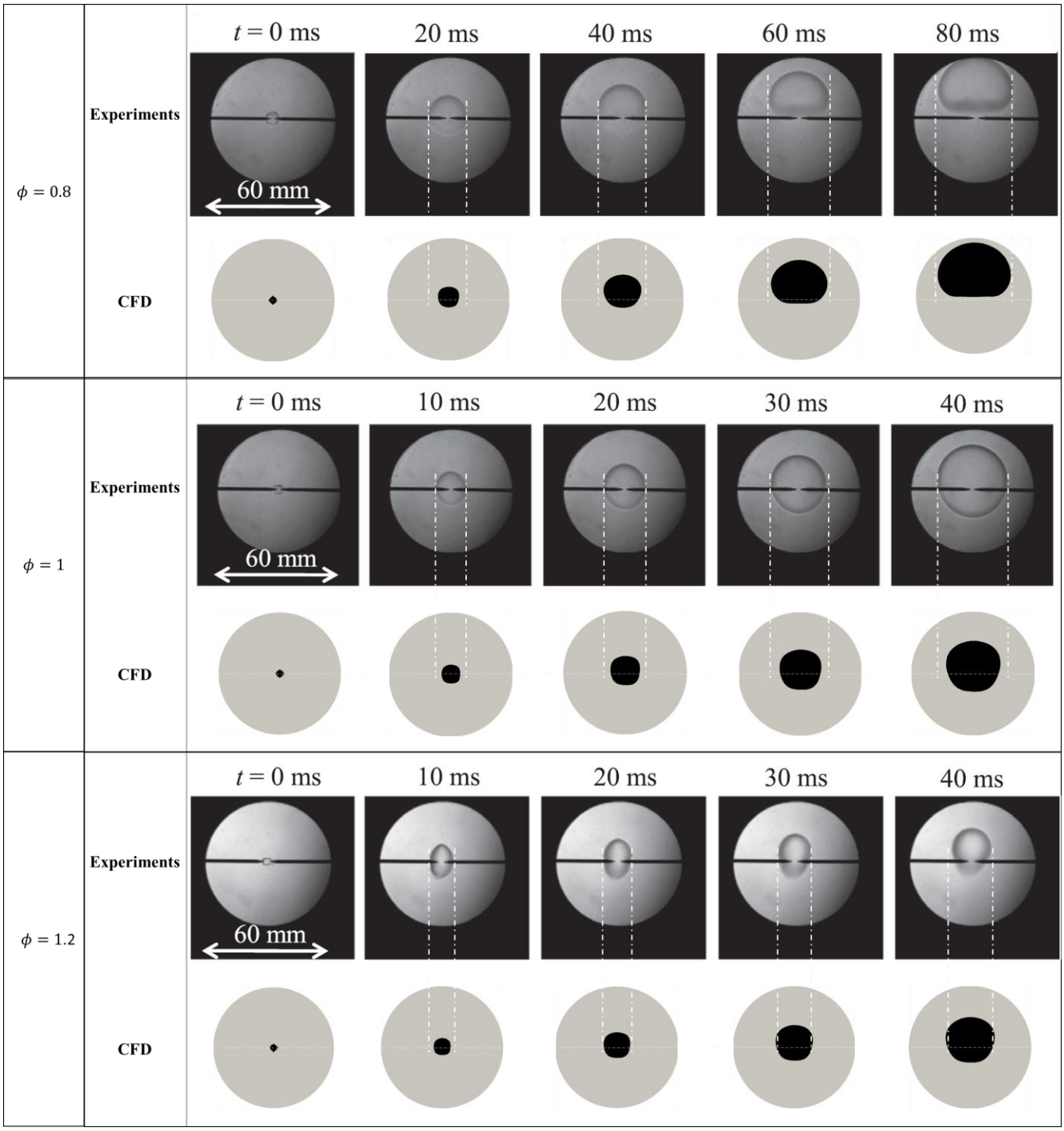

FIGURE 9. VISUAL COMPARISON OF THE FLAME FROM THE EXPERIMENTAL SCHLIEREN IMAGES IN HAYAKAWA ET AL. [2] VS THE CFD RESULTS OBTAINED WITH OTOMO ET AL. [22], FOR AMMONIA/AIR COMBUSTION AT $\phi = 0.8, 1, 1.2$ AT $T = 298\ K$ AND $P = 0.1\ MPa$

Both models, Stagni et al. and Otomo et al. produced very similar results from $\phi = 0.5$ to 5, as shown in FIGURE 12. The comparison with the experimental data by Krejci et al. [31] shows the results to have high accuracy, within the range of uncertainty of the experiments. The models and the experiments are in agreement with the equivalence ratio at which the maximum laminar flame speed is achieved, $\phi = 1.7$. Compared to isooctane and ammonia, where the maximum laminar flame

speed occurs at 1.15 and 1.1, respectively, hydrogen's maximum flame speed occurs under much richer conditions [33]. Nonetheless, the laminar flame speed of hydrogen is much higher than both fuels under the same conditions.

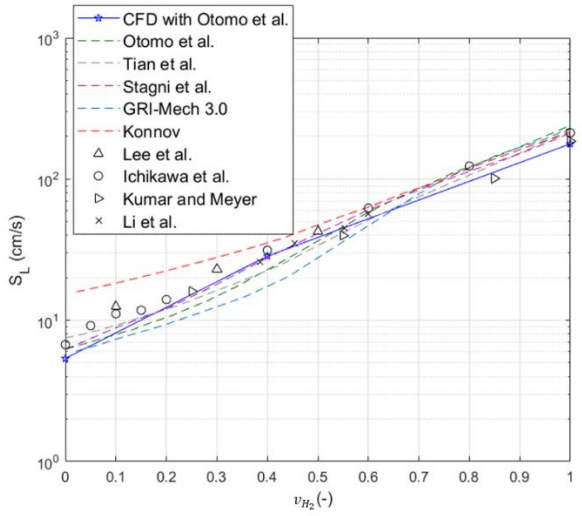

FIGURE 10. LAMINAR FLAME SPEED OF AMMONIA/HYDROGEN/AIR COMBUSTION VS HYDROGEN FUEL VOLUME FRACTIONS (v_{H_2}) AT $\phi = 1, T = 298\ K$ AND $P = 0.1\ MPa$. LINES WITHOUT MARKERS ARE 1-D SIMULATIONS USING OTOMO ET AL. [22], TIAN ET AL. [14], STAGNI ET AL. [23], GRI-MECH 3.0 [30], AND KONNOV [29]. EXPERIMENTS BY LEE ET AL. [32], ICHIKAWA ET AL. [9], KUMAR AND MEYER [33], AND LI ET AL. [34].

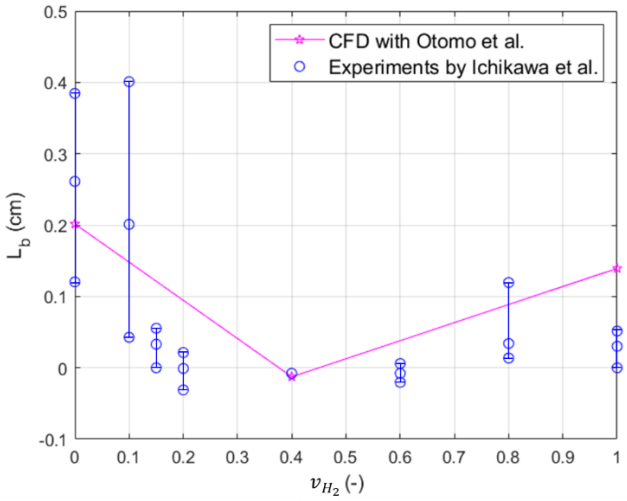

FIGURE 11. BURNT GAS MARKSTEIN LENGTH L_b VS VOLUMETRIC HYDROGEN TO AMMONIA RATIO v_{H_2} COMPARISON OF 3-D CFD RESULTS OBTAINED WITH OTOMO ET AL. [22]AND EXPERIMENTS BY ICHIKAWA ET AL.[9].

FIGURE 13 shows that the autoignition of hydrogen was well predicted by Stagni et al. at higher temperatures, while Otomo et al.'s predictions were more accurate for lower temperatures. A further numerical investigation was done on the effect of the equivalence ratio on the ignition delay time. It can be seen that both models predict an inversion in the effect of ϕ.

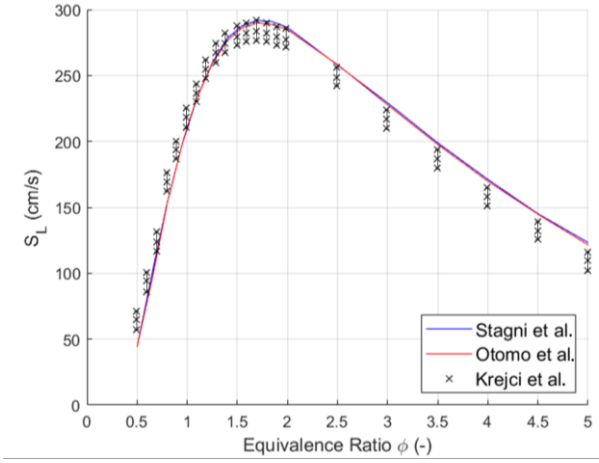

FIGURE 12. HYDROGEN/AIR LAMINAR FLAME SPEED VS EQUIVALENCE RATIO ϕ AT $P = 1\ atm$ AND $T = 298\ K$. 1-D SIMULATIONS USING STAGNI ET AL. [23], AND OTOMO ET AL. [22]. EXPERIMENTS BY KREJCI ET AL. [31].

The models predict the leanest condition to have the fastest autoignition at higher temperatures and the richest condition to have the fastest autoignition at lower temperatures. The temperature of the crossover point is different for each mechanism, but both mechanisms have the same pattern. It is worth mentioning that for ammonia at a similar pressure of 30 atm but a higher temperature range this trend in relative ignition delay with respect to equivalence ratio, as shown in FIGURE 5c, is consistent with the hydrogen autoignition in the upper temperature range.

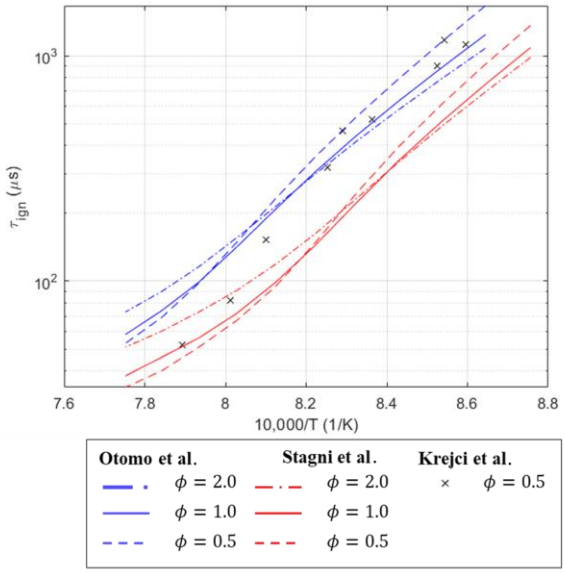

FIGURE 13. IGNITION DELAY TIME τ_{ign} OF PURE HYDROGEN AT $P = 32\ atm$. 0-D SIMULATION USING OTOMO ET AL. [22], AND STAGNI ET AL. [23] AT $\phi = 0.5, 1.0, 2.0$, EXPERIMENT BY KREJCI ET AL. [31] AT $\phi = 0.5$.

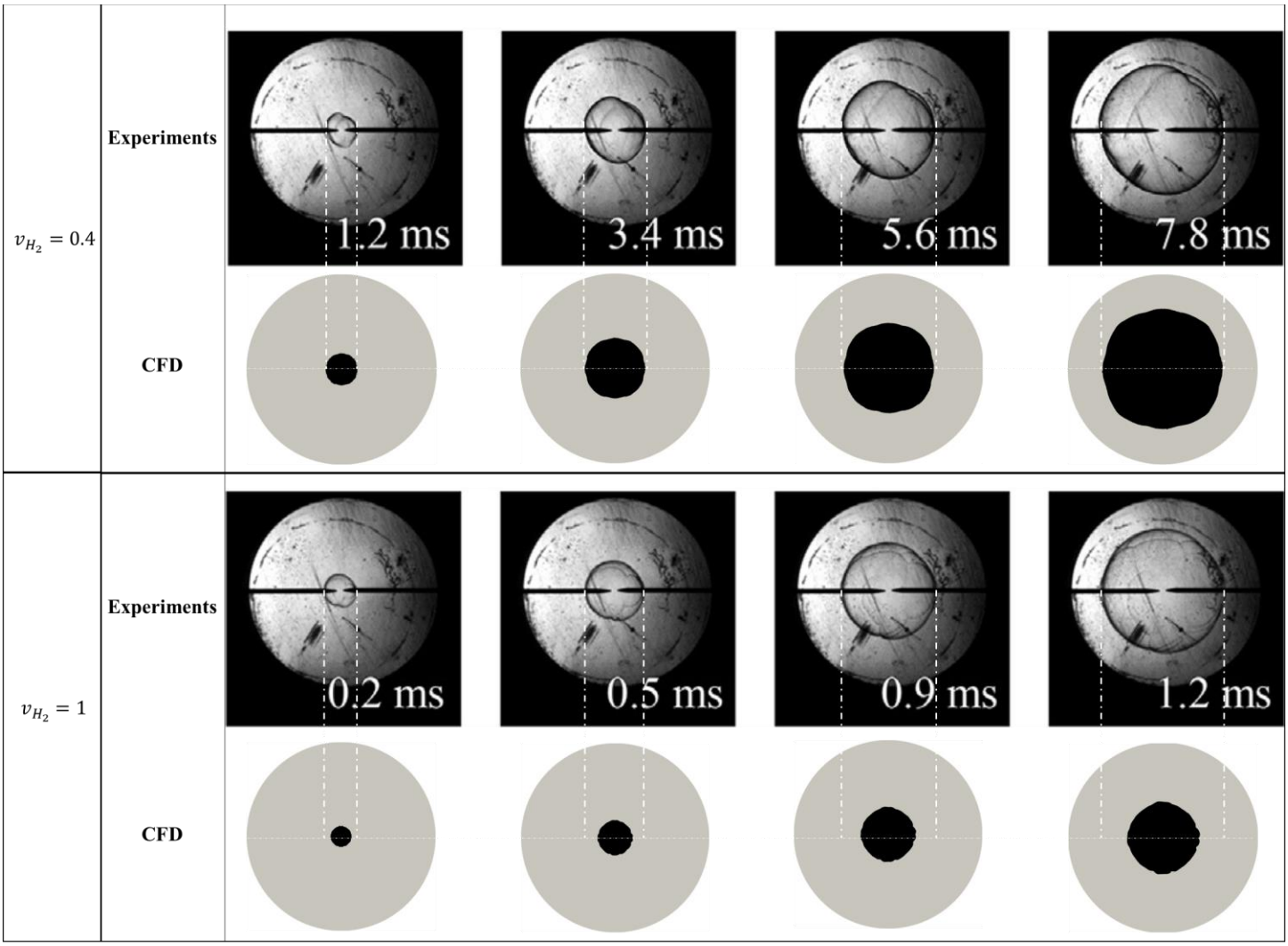

FIGURE 14. VISUAL COMPARISON OF THE FLAME FROM THE EXPERIMENTAL SCHLIEREN IMAGES IN ICHIKAWA ET AL. VS THE RESULTS OBTAINED BY THE CFD FOR AMMONIA/HYDROGEN/AIR COMBUSTION AT $\phi = 1$ AT DIFFERENT AMMONIA:HYDROGEN VOLUMETRIC FUEL CONCENTRATIONS

4. CONCLUSION

The work presented in this study emphasized the importance of using 3-D analysis in understanding the combustion behavior of fuels. The results showed a significant deviation of the laminar flame speed value when applied in a 1-D model and a 3-D model, although the trends of the laminar flame speed vs equivalence ratio and hydrogen:ammonia ratios were consistent with the 1-D model. The stretch rate relation that ties the stretched flame speed with the unstretched flame speed through the Markstein length, was seen to play a major role in that regard. This study also compared the different methods that could be applied to measure the laminar flame speed and the sensitivity of the results to these methods. These methods proved to be pivotal in slow flames where buoyancy has a significant effect. The 0-D analysis of the ignition time delay revealed that ammonia and ammonia/hydrogen can have faster autoignition at lean conditions compared to richer mixtures. This behavior's effects are of great importance in applications like internal combustion engines, and therefore, needs to be better understood and investigated.

In general, ammonia and hydrogen showed that their combustion characteristics are complementary and can be blended to enhance their standalone performance. Ammonia could offer a solution to hydrogen's storage problems and hydrogen could enhance the shortcomings of ammonia in combustion. Therefore, understanding the properties of the blends of these two fuels at different ratios is pivotal to their applications.

ACKNOWLEDGEMENTS

This work was made possible through funding from the U.S. Office of Naval Research under Award No. N00014-22-1-2001. Additionally, the authors would like to thank Stony Brook

Research Computing and Cyberinfrastructure, and the Institute for Advanced Computational Science at Stony Brook University for access to the high-performance SeaWulf computing system, which was made possible by a $1.4M National Science Foundation grant (#1531492).

5. REFERENCES

[1] H. Xiao, A. Valera-Medina, and P. J. Bowen, "Modeling Combustion of Ammonia/Hydrogen Fuel Blends under Gas Turbine Conditions," *Energy and Fuels*, vol. 31, no. 8, pp. 8631–8642, Aug. 2017, doi: 10.1021/acs.energyfuels.7b00709.

[2] A. Hayakawa, T. Goto, R. Mimoto, Y. Arakawa, T. Kudo, and H. Kobayashi, "Laminar burning velocity and Markstein length of ammonia/air premixed flames at various pressures," *Fuel*, vol. 159, pp. 98–106, Jul. 2015, doi: 10.1016/j.fuel.2015.06.070.

[3] C. Zamfirescu and I. Dincer, "Ammonia as a green fuel and hydrogen source for vehicular applications," *Fuel Processing Technology*, vol. 90, no. 5, pp. 729–737, May 2009, doi: 10.1016/j.fuproc.2009.02.004.

[4] W. Wang, J. M. Herreros, A. Tsolakis, and A. P. E. York, "Ammonia as hydrogen carrier for transportation; Investigation of the ammonia exhaust gas fuel reforming," *International Journal of Hydrogen Energy*, vol. 38, no. 23, pp. 9907–9917, Aug. 2013, doi: 10.1016/j.ijhydene.2013.05.144.

[5] H. Kobayashi, A. Hayakawa, K. D. K. A. Somarathne, and E. C. Okafor, "Science and technology of ammonia combustion," *Proceedings of the Combustion Institute*, vol. 37, no. 1, pp. 109–133, 2019, doi: 10.1016/j.proci.2018.09.029.

[6] M. Zavka, "Device for operating internal combustion engines with mixtures of ammonia, hydrogen, and nitrogen prepared from ammonia," 1938

[7] E. Kroch, "Ammonia - a fuel for motor buses," *Journal of the Institute of Petroleum*, no. 31, pp. 213–223, 1945.

[8] E. S. Starkman, H. K. Newhall, R. Sutton, T. Maguire, and L. Farbar, "Ammonia as a Spark Ignition Engine Fuel: Theory and Application," *SAE Transactions*, vol. 75, pp. 765–784, 1967, [Online]. Available: http://www.jstor.org.proxy.library.stonybrook.edu/stable/44563674

[9] A. Ichikawa, A. Hayakawa, Y. Kitagawa, K. D. Kunkuma Amila Somarathne, T. Kudo, and H. Kobayashi, "Laminar burning velocity and Markstein length of ammonia/hydrogen/air premixed flames at elevated pressures," *International Journal of Hydrogen Energy*, vol. 40, no. 30, pp. 9570–9578, Aug. 2015, doi: 10.1016/j.ijhydene.2015.04.024.

[10] B. Lewis and G. von Elbe, *Combustion, Flames and Explosions of Gases*, 3rd ed. London: Academic Press, 1987.

[11] L. Schlapbach and A. Züttel, "Hydrogen-storage materials for mobile applications," *Nature*, vol. 414, no. 6861, pp. 353–358, 2001, doi: 10.1038/35104634.

[12] P. D. Ronney, "Effect of Chemistry and Transport Properties on Near-Limit Flames at Microgravity," *Combustion Science and Technology*, vol. 59, no. 1–3, pp. 123–141, May 1988, doi: 10.1080/00102208808947092.

[13] U. J. Pfahl, M. C. Ross, J. E. Shepherd, K. O. Pasamehmetoglu, and C. Unal, "Flammability limits, ignition energy, and flame speeds in H2–CH4–NH3–N2O–O2–N2 mixtures," *Combustion and Flame*, vol. 123, no. 1, pp. 140–158, 2000, doi: https://doi.org/10.1016/S0010-2180(00)00152-8.

[14] Z. Tian, Y. Li, L. Zhang, P. Glarborg, and F. Qi, "An experimental and kinetic modeling study of premixed NH3/CH4/O2/Ar flames at low pressure," *Combustion and Flame*, vol. 156, no. 7, pp. 1413–1426, 2009, doi: https://doi.org/10.1016/j.combustflame.2009.03.005.

[15] O. Mathieu and E. L. Petersen, "Experimental and modeling study on the high-temperature oxidation of Ammonia and related NOx chemistry," *Combustion and Flame*, vol. 162, no. 3, pp. 554–570, Mar. 2015, doi: 10.1016/j.combustflame.2014.08.022.

[16] J. A. Miller, M. D. Smooke, R. M. Green, and R. J. Kee, "Kinetic Modeling of the Oxidation of Ammonia in Flames," *Combustion Science and Technology*, vol. 34, no. 1–6, pp. 149–176, Oct. 1983, doi: 10.1080/00102208308923691.

[17] A. A. Konnov and J. de Ruyck, "A possible new route for no formation via N2H3," *Combustion Science and Technology*, vol. 168, no. 1, pp. 1–46, 2001, doi: 10.1080/00102200108907830.

[18] H. Nozari and A. Karabeyoğlu, "Numerical study of combustion characteristics of ammonia as a renewable fuel and establishment of reduced reaction mechanisms," *Fuel*, vol. 159, pp. 223–233, Jul. 2015, doi: 10.1016/j.fuel.2015.06.075.

[19] O. A. Powell, P. Papas, and C. B. Dreyer, "Flame structure measurements of NO in premixed hydrogen–nitrous oxide flames," *Proceedings of the Combustion Institute*, vol. 33, no. 1, pp. 1053–1062, 2011, doi: https://doi.org/10.1016/j.proci.2010.06.042.

[20] C. Duynslaegher, H. Jeanmart, and J. Vandooren, "Flame structure studies of premixed ammonia/hydrogen/oxygen/argon flames: Experimental and numerical investigation," *Proceedings of the Combustion Institute*, vol. 32, no. 1, pp. 1277–1284, 2009, doi: https://doi.org/10.1016/j.proci.2008.06.036.

[21] C. Brackmann *et al.*, "Structure of premixed ammonia + air flames at atmospheric pressure: Laser diagnostics and kinetic modeling," *Combustion and Flame*, vol. 163, pp. 370–381, Jan. 2016, doi: 10.1016/j.combustflame.2015.10.012.

[22] J. Otomo, M. Koshi, T. Mitsumori, H. Iwasaki, and K. Yamada, "Chemical kinetic modeling of ammonia oxidation with improved reaction mechanism for ammonia/air and ammonia/hydrogen/air combustion," *International Journal of Hydrogen Energy*, vol. 43, no.

5, pp. 3004–3014, Feb. 2018, doi: 10.1016/j.ijhydene.2017.12.066.
[23] A. Stagni *et al.*, "An experimental, theoretical and kinetic-modeling study of the gas-phase oxidation of ammonia," *Reaction Chemistry and Engineering*, vol. 5, no. 4, pp. 696–711, Apr. 2020, doi: 10.1039/c9re00429g.
[24] Y. Song, H. Hashemi, J. M. Christensen, C. Zou, P. Marshall, and P. Glarborg, "Ammonia oxidation at high pressure and intermediate temperatures," *Fuel*, vol. 181, pp. 358–365, Oct. 2016, doi: 10.1016/j.fuel.2016.04.100.
[25] S. J. Klippenstein, L. B. Harding, P. Glarborg, and J. A. Miller, "The role of NNH in NO formation and control," *Combustion and Flame*, vol. 158, no. 4, pp. 774–789, Apr. 2011, doi: 10.1016/j.combustflame.2010.12.013.
[26] J. A. Miller and P. Glarborg, "Modeling the thermal De-NOx process: Closing in on a final solution," *International Journal of Chemical Kinetics*, vol. 31, no. 11, pp. 757–765, Jan. 1999, doi: https://doi.org/10.1002/(SICI)1097-4601(1999)31:11<757::AID-JCK1>3.0.CO;2-V.
[27] Reaction Design, "ANSYS Chemkin Theory Manual." ANSYS, San Diego, 2015.
[28] K. J. Richards, P. K. Senecal, and E. Pomraning, "Converge." Convergent Science, Madison, WI, 2022.
[29] A. A. Konnov, "Implementation of the NCN pathway of prompt-NO formation in the detailed reaction mechanism," *Combustion and Flame*, vol. 156, no. 11, pp. 2093–2105, 2009, doi: https://doi.org/10.1016/j.combustflame.2009.03.016.
[30] G. P. Smith *et al.*, "GRI-Mech 3.0," *http://www.me.berkeley.edu/gri_mech/*.
[31] M. C. Krejci *et al.*, "Laminar Flame Speed and Ignition Delay Time Data for the Kinetic Modeling of Hydrogen and Syngas Fuel Blends," *Journal of Engineering for Gas Turbines and Power*, vol. 135, no. 2, Jan. 2013, doi: 10.1115/1.4007737.
[32] J. H. Lee, J. H. Kim, J. H. Park, and O. C. Kwon, "Studies on properties of laminar premixed hydrogen-added ammonia/air flames for hydrogen production," *International Journal of Hydrogen Energy*, vol. 35, no. 3, pp. 1054–1064, Feb. 2010, doi: 10.1016/j.ijhydene.2009.11.071.
[33] K. Kumar, J. E. Freeh, C. J. Sung, and Y. Huang, "Laminar flame speeds of preheated iso-octane/O2/N2 and n-heptane/O2/N2 mixtures," *Journal of Propulsion and Power*, vol. 23, no. 2, pp. 428–436, 2007, doi: 10.2514/1.24391.
[34] J. Li, H. Huang, N. Kobayashi, Z. He, and Y. Nagai, "Study on using hydrogen and ammonia as fuels: Combustion characteristics and NOx formation," *International Journal of Energy Research*, vol. 38, no. 9, pp. 1214–1223, Jul. 2014, doi: 10.1002/er.3141.
[35] P. Clavin, "Dynamic behavior of premixed flame fronts in laminar and turbulent flows," *Progress in Energy and Combustion Science*, vol. 11, no. 1, pp. 1–59, 1985, doi: https://doi.org/10.1016/0360-1285(85)90012-7.
[36] V. F. Zakaznov, L. A. Kursheva, and Z. I. Fedina, "Determination of normal flame velocity and critical diameter of flame extinction in ammonia-air mixture," *Combustion, Explosion and Shock Waves*, vol. 14, no. 6, pp. 710–713, 1978, doi: 10.1007/BF00786097.
[37] K. Takizawa, A. Takahashi, K. Tokuhashi, S. Kondo, and A. Sekiya, "Burning velocity measurements of nitrogen-containing compounds," *Journal of Hazardous Materials*, vol. 155, no. 1, pp. 144–152, 2008, doi: https://doi.org/10.1016/j.jhazmat.2007.11.089.
[38] H. Li, L. Yu, X. Lu, L. Ouyang, S. Sun, and Z. Huang, "Autoignition of ternary blends for gasoline surrogate at wide temperature ranges and at elevated pressure: Shock tube measurements and detailed kinetic modeling," *Fuel*, vol. 181, pp. 916–925, Oct. 2016, doi: 10.1016/j.fuel.2016.05.030.
[39] X. He *et al.*, "An experimental and modeling study of iso-octane ignition delay times under homogeneous charge compression ignition conditions," *Combustion and Flame*, vol. 142, no. 3, pp. 266–275, Aug. 2005, doi: 10.1016/j.combustflame.2005.02.014.